In Situ Synchrotron X-ray Diffraction Experiments on Electrochemically Deposited ZnO Nanostructures

ARTICLE *in* THE JOURNAL OF PHYSICAL CHEMISTRY C · SEPTEMBER 2008

Impact Factor: 4.77 · DOI: 10.1021/jp806184z

In Situ Synchrotron X-ray Diffraction Experiments on Electrochemically Deposited ZnO Nanostructures

Bridget Ingham,*,†,‡ Benoit N. Illy,§ Michael F. Toney,‡ Marci L. Howdyshell,‡,|| and Mary P. Ryan§

Industrial Research Limited, 69 Gracefield Road, Lower Hutt, New Zealand, Stanford Synchrotron Radiation Laboratory, 2575 Sand Hill Road, Menlo Park, California 94025, and Department of Materials and London Centre for Nanotechnology, Imperial College London, Exhibition Road, London SW7 2AZ, United Kingdom

Received: July 13, 2008; Revised Manuscript Received: July 29, 2008

We present results of in situ synchrotron X-ray diffraction experiments on electrochemically formed ZnO nanostructured films during their growth on to Au substrates. This allows the evolution of texture to be monitored throughout the deposition process. The results are in good agreement with previous in situ X-ray absorption spectroscopy measurements of growth kinetics and indicate that strong preferred orientation, which is not evident from the microstructure, develops early in the growth process.

Introduction

Zinc oxide (ZnO) is a wide band gap semiconductor that shows promise as a material for many applications including opto-electronics[1] and sensing.[2] It has the ability to form nanostructures of many different shapes and sizes, which change its physical properties due to their large surface-to-volume ratio and anisotropic shape. Electrochemical deposition is one method of producing ZnO nanostructures.[3] This offers many advantages over other physical deposition techniques including: low-temperature processing, controllable deposition, ease of scaling for production, and that electrolytic processing is an established technology. The morphology of the ZnO nanostructures depends on the deposition conditions, such as the electrochemical potential[4] and the concentration of Zn^{2+} in the solution.[5] By varying the solution pH,[6] temperature[4,7] and potential,[8] the deposition rate can also be controlled.

The deposition of ZnO from aqueous solution is a two-step (electro-)chemical reaction. Dissolved oxygen is reduced to produce hydroxide ions (reaction 1) and then the direct deposition reaction of ZnO (eq 2) follows as a result of the pH dependence on its solubility:

$$O_{2(g)} + 2H_2O_{(l)} + 4e^- \rightarrow 4OH^-_{(aq)} \quad (1)$$

$$Zn^{2+}_{(aq)} + 2OH^-_{(aq)} \rightarrow ZnO_{(s)} + H_2O_{(l)} \quad (2)$$

The electrochemical current density monitored during the deposition gives a measure of the hydroxide production reaction (eq 1); however few studies have been performed that are able to directly monitor the ZnO deposition reaction (eq 2). One technique that has been recently utilized is in situ X-ray absorption spectroscopy (XAS), which can *directly* correlate the electrochemical current density with species specific amounts of material deposited.[8−10]

In the present work, we report in situ X-ray diffraction studies of ZnO nanostructured films during the deposition process. ZnO nanostructured films are usually highly oriented. There is still debate as to how the different deposition conditions affect the orientation, and hence the resulting size and shape of the final nanostructures, which may be rods,[4,11−13] plates,[14] or other structures.[15−20] The crystallographic grain size of the films strongly depends on the deposition time; Zhang et al.[21] suggested that the films start to crystallize after one minute and a dense polycrystalline film is formed after 10 min. The lattice constants *a* and *c*, and the *c*/*a* ratio, increase at more positive deposition potentials.[22] The applied potential has been reported as having an influence on the preferential orientation of the films[23,24] however these results are also dependent on the choice of substrate. For films deposited on Au (111) from alkaline solutions with ascorbic acid added (to reduce the pH in the vicinity of the substrate without oxidizing the Au), highly oriented (002) ZnO nanostructures were formed.[25] On (100), (110) and (111) oriented Au single-crystal substrates, ZnO nanostructures deposited from aqueous solution exhibit strong (002) texturing.[26] The question arises as to whether this texture is present from nucleation, or if it develops at a later stage in the deposition. If from nucleation, then one can produce arbitrarily small, textured nanostructures (by using short nucleation times); if the texture develops later then there is a minimum size that must first be reached in order for the orientation of the nanostructure to be useful (e.g., in waveguide applications).

Synchrotron X-ray diffraction (XRD) is a technique that can be used to obtain crystallographic information during the growth of the nanostructures. In this way the development of any preferred orientation in the ZnO nanostructures can be observed. We describe the results of in situ synchrotron XRD experiments and how these can yield information concerning the growth rates and development of texture in electrochemically formed ZnO nanostructures. This complements our earlier work,[8−10] which was not sensitive to the ZnO nanostructure orientation. By following the development of texture as a function of time and combining this with the nanostructure morphology from scanning electron microscopy (SEM), we gain insight into how the texture develops with respect to the nanostructure shape.

* To whom correspondence should be addressed. E-mail: b.ingham@irl.cri.nz.
† Industrial Research Limited.
‡ Stanford Synchrotron Radiation Laboratory.
§ Imperial College London.
|| Current address: Department of Physics, Ohio State University, 191 West Woodruff Avenue, Columbus, OH 43210.

10.1021/jp806184z CCC: $40.75
Published on Web 08/27/2008

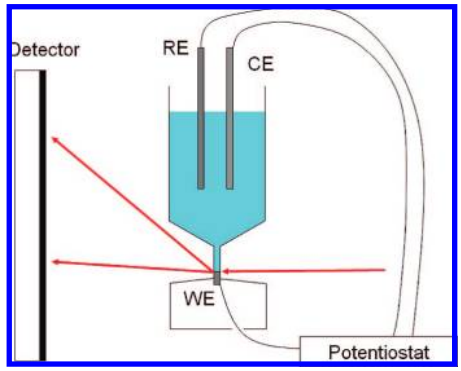

Figure 1. Schematic diagram of experimental setup, showing the electrochemical cell with a Pt counter electrode (CE), Ag/AgCl reference electrode (RE), and quartz rod coated with Au which acts as the working electrode (WE) and sample surface. The arrows represent the X-ray path. There is a maximum angle in the vertical direction that diffracted X-rays can be observed, due to the shape of the cell.

Experimental Section

$Zn(NO_3)_2$ (Riedel DeHaën, 98%) was dissolved in deionized water at 5 mM concentration. The solution also contained a supporting electrolyte (KCl or $CaCl_2$) at 0.1 M concentration. A Pt wire counter electrode and an Ag/AgCl/KCl (3.5 M) reference electrode were used (+0.205 V vs NHE).[27] The solution was held at a constant temperature (65−70 °C) and oxygen gas was bubbled at a moderate rate (2−5 $mL.min^{-1}$) through the solution throughout the deposition. The electrochemistry was controlled with a Gamry PCI4/300 potentiostat. XRD experiments were conducted in situ using a custom-made cell on beam line 11-3 at the Stanford Synchrotron Radiation Laboratory. The beam size was 0.15 mm (horizontal) × 0.05 mm (vertical) and the wavelength 0.9736 Å. A LaB_6 powder standard was used for calibration. The substrate was a quartz rod covered with 150 nm of sputtered, (111) textured Au; this was positioned in a grazing-incidence geometry with a 2 mm X-ray path length through the solution at the base of the cell and acted as the working electrode. Diffracted X-rays were detected with an MAR345 image plate. Images were taken every 1.5−2 min (10 s to collect and 1.5 min for the detector to read out) in a sequence, with two scans recorded before the potential was applied. A diagram of the cell is shown in Figure 1. SEM images were obtained using a LEO 1525 field-emission scanning electron microscope.

Results and Discussion

Figure 2 shows electron micrograph images of a series of ZnO nanostructured films deposited for different times under the same conditions, illustrating the nucleation and later growth of the nanostructures. At the longer times the hexagonal motif of the ZnO crystal structure is apparent; however, this is not so for the images corresponding to the shortest times (<1 min). The question naturally arises as to whether the development of texture accompanies the development in morphology, or not, as this cannot be assessed from the morphology.

The diffraction data collected exhibit arcs corresponding to diffraction from the ZnO nanostructures and the underlying Au electrode film, as the example in Figure 3 shows. (The arcs appear tilted from the normal because the substrate was tilted laterally about the beam.) As the deposition progressed, the ZnO peak intensities increased, corresponding to the amount of (crystalline) material directly deposited. The width of the arcs indicate the degree of texture present in the nanostructures. At the shortest times where ZnO peaks could be observed (1−2 min), the arcs had finite width that did not change with time. Therefore the final texture is present from the earliest measurable times throughout the deposition, even at times where the SEM images do not exhibit any obvious morphology.

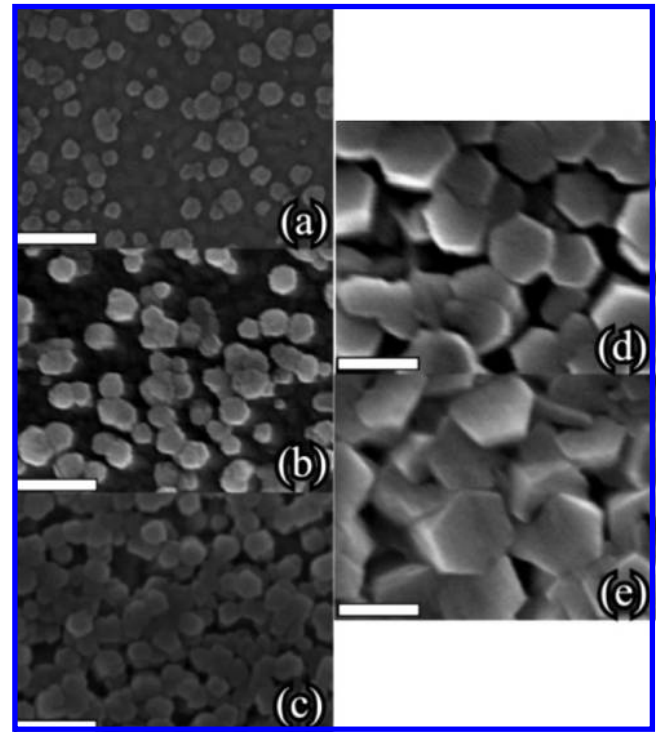

Figure 2. SEM micrographs of ZnO films for different deposition durations: (a) 15 s, (b) 1 min, (c) 4 min, (d) 10 min and (e) 45 min. The deposition solution was 5 mM $Zn(NO_3)_2$ with 0.1 M $CaCl_2$ electrolyte. The potential was −0.67 mV. Scale bar: 200 nm. These depositions were performed in a different cell from that used for the in situ diffraction, but the trends are the same in both cells.

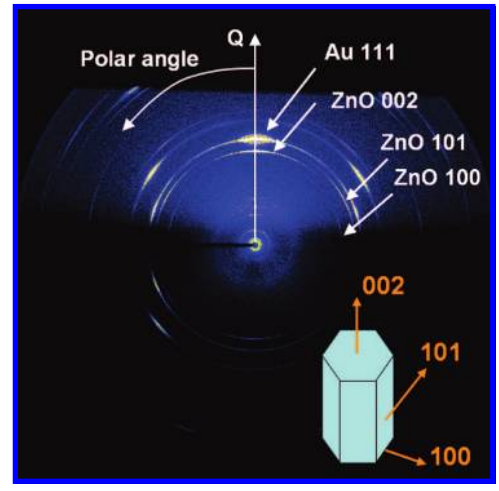

Figure 3. Raw data collected at the end of deposition showing the primary ZnO reflections. The Au (111) peak from the substrate is also identified.

Analysis of the time series data was performed as follows. The data were converted from Cartesian to radial coordinates, so that the data can now be analyzed in terms of Q, the magnitude of the scattering vector, and the polar angle, between the scattering vector and the sample normal (indicated in Figure 3). The peaks in polar angle can then be analyzed at constant Q; akin to performing a chi scan with a point detector.

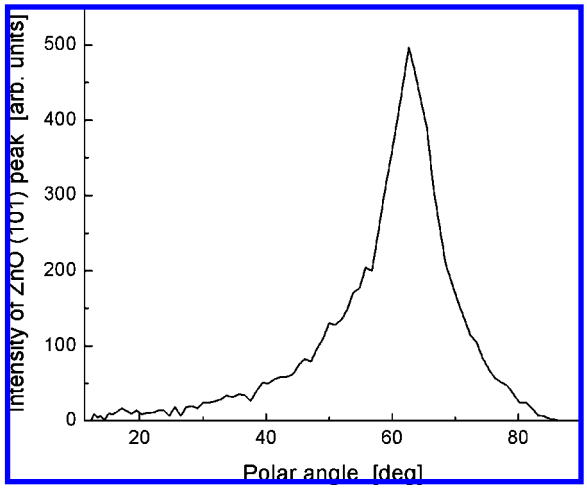

Figure 4. Intensity versus polar angle for the ZnO (101) reflection at the end of a deposition.

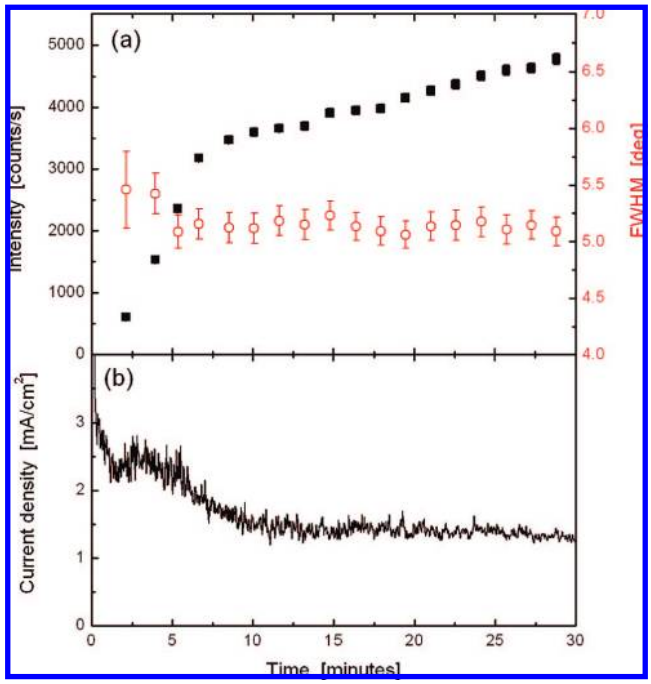

Figure 5. (a) Peak intensity (black closed squares) and full width at half-maximum (fwhm; red open circles), and (b) electrochemical current density, as a function of time during the deposition. The experimental parameters are: 5 mM $Zn(NO_3)_2$, 0.1 M $CaCl_2$ electrolyte, deposition potential −0.67 V, solution temperature 65 °C.

Figure 4 shows an example: the intensity as a function of polar angle for the ZnO (101) peak of a sample at the end of deposition ($E = -0.97$ V). The (101) is the preferred reflection for the analysis as opposed to the (002) or (100) since (a) it is a low order peak and so is not at a high enough angle to be blocked by the finite size of the cell (see Figure 1); (b) given the grazing incidence, the (002) is unfavorable since this is a specular peak and the reflection is not indicative of the true intensity and texture; (c) the (100) is in-plane so once again is not indicative of the true intensity and texture, since no intensity can be measured at $\chi = 90°$ in the grazing incidence geometry. The (101) polar angle plots were fitted with a Lorentzian peak function, averaged, and the area and peak width plotted as a function of time as shown in Figure 5.

The peak area as a function of time (Figure 5a, black closed squares) increases in a manner similar to that observed previously with in situ X-ray absorption spectroscopy.[8,9] There are two regions of the curve: the initial nucleation regime where material is being deposited rapidly; followed by continuous growth at a slower rate which we have previously attributed to continued growth of coalesced structures once the nanostructures become compacted.[8] This trend is also reflected in the current density (Figure 5b), which is initially large and then drops to a constant value. The azimuthal peak width as a function of time (Figure 5a, red open circles) shows no significant change (within the uncertainties), providing quantitative proof that the texture originates during the nucleation. The absolute value of the current density is slightly different to the previous X-ray absorption spectroscopy experiments,[8] owing to the different geometry being used in each case. In the diffraction experiments, the cell is only 2 mm wide in the vicinity of the working electrode, whereas for the X-ray absorption experiments the electrode is open. The deposition reaction is limited by diffusion, and so the reaction rate is decreased in the diffraction experiments.

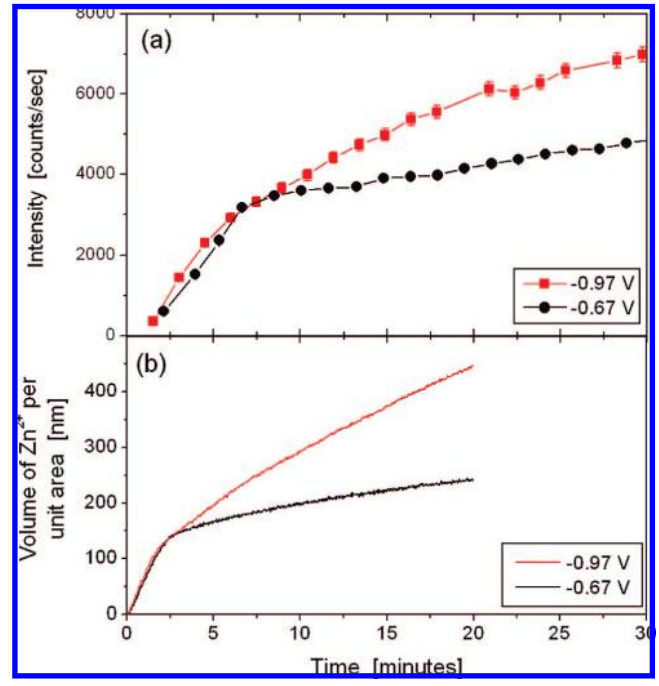

Figure 6. Intensity as a function of time from (a) the present X-ray diffraction results and (b) previous X-ray absorption spectroscopy results, for films deposited from 5 mM $Zn(NO_3)_2$ solution with 0.1 M $CaCl_2$ electrolyte at 65 °C at −0.97 V (red) and −0.67 V (black).

Figure 6a shows the peak area as a function of time for two samples deposited under different conditions which exhibit different growth behavior.[8] At high deposition potentials (−0.67 V), the nucleation stage is prolonged and there is a definite change in the growth rate once the electrode is covered (as indicated by the change in slope in Figure 6a and b). At lower potentials (−0.97 V), the nucleation period is rapid (instantaneous) and the change in growth rate (slope) is more continuous. Figure 6b shows the excellent comparison with previous X-ray absorption spectroscopy results for films formed under the same conditions.[8] Qualitatively the behavior is the same; the slight difference in the time-scale is due to the different geometry used for each experiment. In addition, the azimuthal full-width at half-maximum (fwhm) of the diffraction peak is the same value and constant (5° in polar angle) for both throughout their respective time series.

To further explore the texture of the nanostructures at the earliest deposition times, a series of samples were prepared for

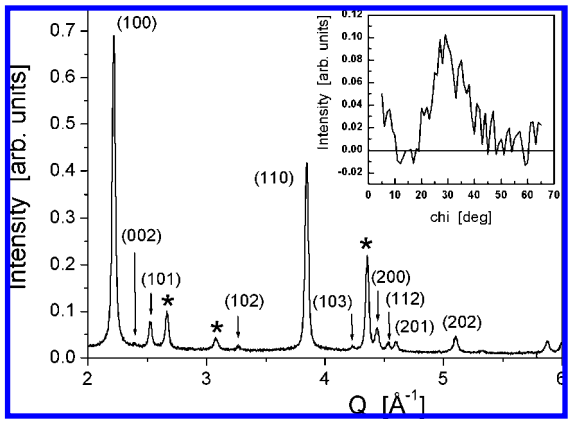

Figure 7. Grazing incidence X-ray diffraction scan for a film deposited for 15 s from a 5 mM $Zn(NO_3)_2$ solution with 0.1 M KCl electrolyte, applied potential −0.67 V. The ZnO peaks are identified by their Miller indices; Au substrate peaks are marked by *. Inset: Polar angle (χ) scan of the ZnO (101) peak.

ex situ measurements. These had the potential applied for 15, 30, and 60 s and hence according to the plots in Figures 2 and 6 correspond to a region where individual nanostructures are initially deposited and are growing quickly. A grazing-incidence radial scan for the sample deposited for 15 s (from a 5 mM $Zn(NO_3)_2$, 0.1 M KCl solution, at an applied potential of −0.67 V) is shown in Figure 7. The peaks observed correspond solely to ZnO and the Au substrate. The respective polar angle (chi) plot for the ZnO (101) peak is shown in the inset (with background subtracted). There is a peak in this plot, which again indicates that at 15 s there is texture present in the nanostructures. The fwhm is 12°, which, compared with Figure 5, indicates the texture increases after the nucleation stage. (The rise in signal as polar angle approaches zero is due to both the signal and background dropping off.)

The continued growth of ZnO into nanorods results from anisotropic growth which is due to the large differences in surface energies of the ZnO crystal faces relating to the polarity of the <002> facet with respect to the <100> and <110> facets of the ZnO wurtzite structure.[28] Deposition occurs preferentially on the <002> surface, most notably when the supply of Zn^{2+} is limited.[4] In the present work, the current density during the electrodeposition is high (see Figure 5) and thus above the limiting diffusion current of zinc ions.[29] The orientation of these rods perpendicular to the substrate is determined in the first few seconds of deposition, during the nucleation stage. Microscopic observation of the incipient crystallites do not show any clear evidence of crystallographic texture; however the XRD data show a strong orientation effect at even short deposition times. Therefore, (a) there is no minimum size below which there is no texture, and (b) the microstructure cannot be used as an indicator of the absence of texture at small nanostructure sizes. This shows that it is possible to produce arbitrarily small, textured nanostructures for use in devices such as in waveguides.

Conclusion

The question of the evolution of texture in the electrochemical deposition of ZnO nanostructures has been investigated using in situ X-ray diffraction. The nuclei are textured in the (002) direction, and this then propagates through the crystallites as the nanostructures grow. Texture is observed in ex situ samples deposited for short times (in the nucleation region), even though the microstructure does not suggest it, and has also been followed in situ through the ensuing growth process. Given that the texture that develops during the nucleation event goes on to affect the texture and morphology of the final film, in principle the final morphology can be altered by simply tuning the nucleation conditions.

Acknowledgment. XRD data were collected at beam line 11-3 at the Stanford Synchrotron Radiation Laboratory, a national user facility operated by Stanford University on behalf of the U.S. Department of Energy, Office of Basic Energy Sciences. XAS data were collected at beam line X10C at the National Synchrotron Light Source. Use of the NSLS, Brookhaven National Laboratory, is supported by the U.S. Department of Energy, Office of Basic Energy Sciences. The authors thank H. Isaacs, K. Sutter, L. Fareria and M. Sansone at NSLS and BNL for technical support. Funding was provided in part by the New Zealand Foundation for Research, Science and Technology under Contract No. CO8X0409. M.L.H. was supported by a Science Undergraduate Laboratory Internship, funded by the U.S. Department of Energy.

References and Notes

(1) Law, M.; Greene, L. E.; Johnson, J. C.; Saykally, R.; Yang, P. D. *Nat. Mater.* **2005**, *4*, 455.
(2) Wan, Q.; Li, H.; Chen, Y. J.; Wang, T. H.; He, X. L.; Li, J. P.; Lin, C. L. *Appl. Phys. Lett.* **2004**, *84*, 3654.
(3) Wong, M. H.; Berenov, A.; Qi, X.; Kappers, M. J.; Barber, Z. H.; Illy, B.; Lockman, Z.; Ryan, M. P.; MacManus-Driscoll, J. L. *Nanotechnology* **2003**, *14*, 968.
(4) Peulon, S.; Lincot, D. *J. Electrochem. Soc.* **1998**, *145*, 864.
(5) Izaki, M.; Omi, T. *J. Electrochem. Soc.* **1996**, *143*, L53.
(6) Fahoumea, M.; Maghfoula, O.; Aggoura, M.; Hartitib, B.; Chraibic, F.; Ennaouic, A. *Solar En. Mat. Solar Cells* **2006**, *90*, 1437.
(7) Goux, A.; Pauporte, T.; Chivot, J.; Lincot, D. *Electrochim. Acta* **2005**, *50*, 2239.
(8) Ingham, B.; Illy, B. N.; Ryan, M. P. *J. Phys. Chem. C* **2008**, *112*, 2820.
(9) Ingham, B.; Illy, B. N.; Mackay, J. R.; White, S. P.; Hendy, S. C.; Ryan, M. P. *Mater. Res. Soc. Symp. Proc.* **2007**, *1017*, DD12–16.
(10) Ingham, B.; Illy, B. N.; Ryan, M. P. *Curr. Appl. Phys.* **2008**, *8*, 455.
(11) Wang, X.; Song, J.; Wang, Z. L. *J. Mater. Chem.* **2007**, *17*, 711.
(12) Yang, J.; Liu, G.; Lu, J.; Qiu, Y.; Yang, S. *Appl. Phys. Lett.* **2007**, *90*, 103109.
(13) Yu, H.; Zhang, Z.; Han, M.; Hao, X.; Zhu, F. *J. Am. Chem. Soc.* **2005**, *127*, 2378.
(14) Illy, B.; Shollock, B. A.; MacManus-Driscoll, J. L.; Ryan, M. P. *Nanotechnology* **2005**, *16*, 320.
(15) Vayssieres, L. *Adv. Mater.* **2003**, *15*, 464.
(16) Cao, B.; Li, Y.; Duan, G.; Cai, W. *Cryst. Growth Design* **2006**, *6*, 1091.
(17) Yang, P.; Yan, H.; Mao, S.; Russo, R.; Johnson, J.; Saykally, R.; Morris, N.; Pham, J.; He, R.; Choi, H. J. *Adv. Func. Mater.* **2002**, *12*, 323.
(18) Yu, L.; Zhang, G.; Li, S.; Xi, Z.; Guo, D. *J. Cryst. Growth* **2007**, *299*, 184.
(19) Yu, K.; Jin, Z.; Liu, X.; Zhao, J.; Feng, J. *Appl. Surf. Sci.* **2007**, *253*, 4072.
(20) Tang, Y.; Luo, L.; Chen, Z.; Jiang, Y.; Li, B.; Jia, Z.; Xu, L. *Electrochem. Commun.* **2007**, *9*, 289.
(21) Zhang, Y.; Weng, J.; Zhang, Y.; Xu, L.; Xu, J.; Huang, X.; Chen, K. *Physica E* **2005**, *27*, 183.
(22) Marotti, R. E.; Guerra, D. N.; Bello, C.; Machado, G.; Dalchiele, E. A. *Solar En. Mater. Solar Cells* **2004**, *82*, 85.
(23) Dalchiele, E. A.; Giorgi, P.; Marotti, R. E.; Martin, F.; Ramos-Barrado, J. R.; Ayouci, R.; Leinen, D. *Solar En. Mater. Solar Cells* **2001**, *70*, 245.
(24) Izaki, M.; Omi, T. *Appl. Phys. Lett.* **1996**, *68*, 2439.
(25) Limmer, S. J.; Kulp, E. A.; Switzer, J. A. *Langmuir* **2006**, *22*, 10535.
(26) Liu, R.; Vertegel, A. A.; Bohannan, E. W.; Sorenson, T. A.; Switzer, J. A. *Chem. Mater.* **2001**, *13*, 508.
(27) All potentials discussed herein are given vs Ag/AgCl/KCl (3.5 M) reference electrode.
(28) Li, W. J.; Shi, E. W.; Zhong, W. Z.; Yim, Z. W. *J. Cryst. Growth* **1999**, *203*, 186.
(29) Pauporté, Th.; Lincot, D. *J. Electroanal. Chem.* **2001**, *517*, 54.

JP806184Z